International Journal of Mass Spectrometry 300 (2011) 182–193

Contents lists available at ScienceDirect

International Journal of Mass Spectrometry

journal homepage: www.elsevier.com/locate/ijms

Ionization of vapor molecules by an electrospray cloud

Juan Fernandez de la Mora*

Yale University, Department of Mechanical Engineering, PO Box 208286, 9 Hillhouse Avenue, New Haven, CT 06520-8286, United States

ARTICLE INFO

Article history:
Received 6 May 2010
Received in revised form 27 August 2010
Accepted 8 September 2010
Available online 17 September 2010

Keywords:
Vapor
Gas phase ionization
API
Charge exchange
Recombination
Ionization probability

ABSTRACT

We first summarize the early work by Fenn and colleagues on vapor ionization by an electrospray cloud (subsequently dubbed secondary electrospray ionization, or SESI), followed by analysis via an atmospheric pressure ionization mass spectrometer (API-MS). It was in part reported in Ph.D. theses and presented to ASMS conferences, but remains largely unpublished. After spending 20 years in limbo, various aspects of their method have begun to be used, leading recently to outstanding limits of detection of ambient volatiles (parts per quadrillion; ppq). There is still much room for improvement of the method, as the ionization probability (defined as the concentration ratio n_s/n_v between ionized vapor and neutral vapor) is $p \sim 10^{-3}$–10^{-4}. This result follows from recent approximate measurements, as well as from a newly derived expression for the equilibrium value p_e under space charge dominated conditions typical of an ES cloud (probably also of a corona discharge): $p_e = k\varepsilon_o/(Z_s q)$. This simple expression is derived from a balance between space charge dilution ($dn_s/dt = -Z_s n_s n_i q/\varepsilon_o$) and the rate of ionization of neutral vapor ($dn_s/dt = k n_v n_i$). It is independent of the concentration n_i of the charging drops (or ions), but depends on the electrical mobility Z_s of the ionized vapor and the net charge q on the charging species (ions or drops). ε_o is the electrical permittivity of vacuum. Still unresolved is the important mechanistic issue of whether the charge-exchange rate coefficient k corresponds to vapor collisions with ES drops (k_d), or rather with individual ions formed after complete drop evaporation (k_p, based on the ion-induced-dipole interaction model). Coincidentally, an upper limit obtained for k_d is comparable to k_p. The ionization efficiency of SESI is compared to that of radioactive and corona sources. Appendices include information on the various rate coefficients fixing p_e. They extend the ion-induced-dipole interaction model to account for the relatively large size of most vapor molecules of interest. Size effects on k_p are found to be modest, in contrast with the strong size dependence of the mobility of large ions.

1. Introduction

John Fenn's work with molecular beams did not earn him a royal dinner in Stockholm. But it did so for three of his chemist friends,[1] providing early signs of the now better appreciated fact that it pays to follow Fenn closely. Indeed, his outstanding creativity and insights have been manifest not only through his scientific work, but also in informal conversations, seminar discussions; unpublished conference abstracts, patents, and grant applications and reports. Fenn has recognized many of his ideas as important, but he has always had far more than he could personally handle. No wonder, as just to get ESI standing on its own feet took him from 1968 to 1988. I had the good fortune of sharing Mason lab with John as a graduate student (1977–1980) and as a colleague (1981–1993). I followed him closely first on the subject of gas mixtures with disparate masses (the heart of the seeded molecular beam [2,3], and then onto electrospray atomization. Among the scientific subjects I have pursued, I find it hard to identify any without substantial Fennish roots. Since John's contributions to the ionization of *involatile* species are well known, I will presently discuss electrospray ionization of *volatile* species, my most recent borrowing from his intellectual overstock [4–6]. Fenn and colleagues have not yet published on it, so it is appropriately introduced through the following quotation [4]:

> *At the 34th (1986) ASMS Conference we reported that: "On several occasions strange peaks in observed ESPI mass spectra have been traced to contaminants in the nitrogen bath gas. To elucidate these observations we have effected deliberate contamination of the bath gas by injecting small quantities of such species as acetone, dioxane, methyl amine and tri-ethylene glycol. Strong peaks comprising protonated parent molecules were obtained even at a concentration level estimated at ppb..When..(the sprayed methanol-water mixture contained even greater amounts of the*

* Corresponding author. Tel.: +1 203 432 4347; fax: +1 203 432 7654.
E-mail address: juan.delamora@yale.edu.

[1] The following quotation is from Dudley's R. Herchbach's [1] Nobel lecture: *Like many others since, our adoption of supersonic nozzles was spurred by John Fenn and Jim Anderson, ardent evangelists among the chemical engineers then exploring fluid flow in nozzles.*

1387-3806/$ – see front matter © 2010 Elsevier B.V. All rights reserved.
doi:10.1016/j.ijms.2010.09.009

same materials)..no corresponding peaks were found in the resulting spectra. We concluded that the ionization mechanism must involve charge exchange or chemi-ionization interactions between gas phase molecules and charged species produced in the ES process." [5] *In later experiments some species at ppb levels or less in the counter current drying gas produced ions identical with those from the same species as solutes in the sprayed solution. We concluded that in those later experiments the gas phase molecules were collected by ES droplets, then emitted as ions as the droplet evaporated just as if they had been solutes in the sprayed solution. It seems likely that in the earlier results the droplets had already evaporated before they came in contact with the "contaminants" in the bath gas. Recently, in exploring mobility analysis for ES ions Hill et al.* [7] *rediscovered this phenomenon, dubbing it "Secondary Electrospray Ionization" or SESI and attributing it to gas phase proton exchange between ES ions of small solutes and neutral molecules, as we did in our first experiments. Hill et al also suggested that gas phase interactions between ES droplets and neutral molecules might provide even more effective ionization, i.e. the mechanism we assumed in our later studies*.

The Fenn proposal for gas analysis had two main components. The first was to ionize the vapors at atmospheric pressure with an electrospray cloud. The second was to analyze them in a mass spectrometer with an atmospheric pressure source (API-MS).

1.1. API-MS in volatile analysis

Mass spectrometry (MS) has long been an established technique for gas (and vapor) analysis, where the gas is first introduced into the vacuum system of the MS, and ionized at reduced pressure, most often by electron impact (EI). EI leads to substantial molecule fragmentation, which complicates the recognition of the multiple species typically contained in complex samples. For this reason, prior separation by gas chromatography (GC) has been widely adopted. GC–EI-MS then provides a powerful tool for gas analysis, where the complex fingerprint of the EI spectrum is exploited for species identification. Faster gas analysis directly from moderately complicated samples is also possible (without GC) via milder low pressure chemical ionization techniques producing less fragmentation. GC–MS systems typically use small flows of sample gas, having therefore modest pumping requirements and moderate costs. Similar GC and MS instrumentation has also been used in conjunction with atmospheric pressure chemical ionization APCI, relying on either a ^{63}Ni radioactive source, or a corona discharge [8–10]. This early APCI work used very small orifices (~25 μm) to sample a minute flow rate (~0.0057 l/min) of atmospheric pressure gas into the MS. Under such conditions, the supersonic free jet expanding into the vacuum has a modest Reynolds number (~570), so that condensation of the expansion-cooled vapors on the ions is generally not a problem. However, as the flow rate of sample gas grows into the range of 0.1–1 l/min, the situation changes, and a rather different atmospheric pressure interface needs to be developed to avoid vapor condensation on ions [11]. This type of mass spectrometer, often referred to as an atmospheric pressure ionization mass spectrometer (API-MS) first came into being along two different research lines. Following the early work of French and colleagues [12,13], Thomson et al. [14] used it to study the mechanism for ion formation from evaporating drops. The original technique was commercialized by Sciex for gas analysis [15]. The second development was by Fenn and colleagues [16–20], and led to electrospray ionization (ESI) MS. Both approaches avoided the condensation problem by interposing a stream of dry gas between the sampling orifice of the mass spectrometer and the sample gas, so that the ion–gas mixture brought into the vacuum system was dry. An alternative solution practiced in so-called thermospray (TS) [21] and later implemented in several commercial ESI sources ingests the humid gas from the source and controls free jet vapor condensation via substantial heating. Once API-MS and ESI became widely used, this type of mass spectrometer evolved so drastically as to become only remotely connected to the early instruments of Horning et al. [8]. In particular, ion guides [22] have led to ion transmission and detection efficiencies from the atmospheric source to the detector as high as 12% [23] and even 20% [24]. The broad exploitation of API-MS for gas analysis seemed then only natural. However, for a long time, API-MS had very little impact on gas analysis. As reviewed by Covey et al. [25], even the preexisting niche applications following from Sciex's trace atmospheric gas analysis (TAGA) and its implementation for cargo screening faded away. The simpler and more economical GC–MS remained the main approach to gas analysis, while API-MS was coupled primarily to liquid chromatography [26]. The use of API (either SESI or corona discharge) for gas analysis nonetheless stayed alive in a few studies, most often in connection to GC [27–31]. In most of these investigations a solution was injected in the GC, giving lowest detection levels (LDL) of 6×10^{12} molecules [27], 2.4×10^{10} molecules [29], and 0.71×10^{10} molecules [31]. GC–APCI-MS analysis has recently been used for relatively rapid (~15 min) analysis of volatile metabolites from cultured bacteria, showing lowest detection limits of 17 pg for indole (8.7×10^{10} molecules) [30]. We have followed more closely the Fenn approach, producing gas phase standards of known concentration, ionizing them by SESI, and going directly to the API-MS without GC [32–34]. Interestingly, this substantially faster approach is able to cope with complex media such as emanations from breath [32] and skin [33]. In the case of explosives, it has shown unusually low limits of detection (LOD), initially 0.2 ppt (10^8 molecules) [34], and more recently 5 ppq (6.25×10^6 molecules, or 10^{-13} g of RDX) [35]. The potential anticipated by Fenn is therefore evolving rapidly. The large number of molecules still required for detection is presently dictated by two factors. One is the relatively low vapor ionization probability observed ($p \sim 10^{-4}$), to which we shall devote some serious attention here. The other is chemical noise, still demanding of the order of 10^3 ions for detection. Recent noise reduction efforts have been based on increasing the resolving power of triple quadrupoles via prior ion mobility spectrometry [36–39]. The approach is quite natural: once one decides to generate the ions in a gas at atmospheric pressure, it makes sense to separate them in that gas prior to mass analysis.

1.2. Vapor ionization based on an ES cloud

As noted in the long passage by Fenn and colleagues quoted earlier, the term secondary ESI (SESI) was introduced by Hill and colleagues [40–43] to distinguish the ionization of species originally in a gas *external to the sprayed liquid*, from conventional ESI of an analyte originally dissolved in the sprayed liquid. A number of ESI-based ionization methods have been introduced following the invention of desorption ESI (DESI) [44]. Although DESI was designed for analysis of condensed substances deposited on a surface (other than the drop surface), its variants not involving a surface are hard to distinguish from SESI [34] and will not be discussed separately here. Hill and colleagues have devoted three detailed studies to SESI, whose invention they trace to a 1994 article [40], unaware of the precedents from Fenn's group. They confirm several of the earlier mechanistic findings, and add numerous new results. They report that the sensitivity of SESI and a corona source are comparable to each other and an order of magnitude higher than that of a ^{63}Ni source [43]. This later result is probably circumstantial to their experiment, because Carroll et al. [9] had concluded that corona and ^{63}Ni ionization at atmospheric pressure are similarly sensitive at low vapor concentration (though the larger ion currents associ-

ated to the discharge extended the linear response to higher vapor concentrations). These SESI studies [40–43] were primarily centered on ion mobility spectrometry (IMS). Therefore, although they made × use of a mass spectrometer downstream of the IMS, the overall sensitivity is far below that possible based on contemporary commercial API-MS systems. Conclusions on the vapor sensitivity achievable by SESI-API-MS are therefore difficult to draw from this work.

1.3. Advantages of API-MS detection of volatiles and recent applications

We have already noted the spectral simplicity benefit of all three forms of API of volatiles over EI. This advantage is restricted to sufficiently polar species capable of retaining a charge at atmospheric pressure, while EI is effective also for nonpolar vapors. Also, EI can be substituted by chemical ionization (CI), also taking place at reduced pressure, but producing ions more closely related to the original neutral. The advantage of API in terms of sensitivity is apparently not due to differences in ionization efficiency of the vapor, which is $\sim 10^{-4}$ for EI as well as for SESI [34]. The real advantage of API-MS derives mainly from the very high ion transmission efficiencies achieved by contemporary instruments, and by the typically much larger sample flow rates taken (3 l/min in Sciex API-5000 triple quadrupole versus 0.0057 l/min in [8]). This sensitivity gain comes of course at a cost, both in terms of portability and capital investment. Another advantage of API-MS instruments is that, because ionization takes place at atmospheric pressure, the ions can be separated by their mobility prior to mass analysis in FAIMS devices [36,37] (also referred to as DMS [38]), as well as in differential mobility analyzers (DMAs [39]). Excellent resolution and ion transmission have been reported for DMS-MS when using polar vapor additives [38]. Also with a DMA using dry air coupled to Sciex's API 3000 triple quadrupole [39b]. The latter study reports an example of an analyte spiked in a matrix as complex as urine, where mobility selection with a DMA was as effective as liquid chromatography (LC) in removing background, even though the DMA operates orders of magnitude faster than LC.

The main issues addressed in the rest of this paper relate to the effectiveness of SESI as an ionizer for vapor species, and its relative merits with respect to alternative sources. This task will be facilitated by newly derived theoretical limits for the ionization probability in a space-charge limited situation.

2. The equilibrium ionization probability p_e

We shall consider two situations. The first, the *neutral plasma*, is representative of a bipolar ionic atmosphere where approximately as many positive and negative ions coexist after being formed by dissociation of a neutral gas by ionizing radiation (α, β, ultraviolet light, X rays, etc.) in the absence of intense electric fields. A common *neutral plasma* would be formed by a ^{63}Ni source. The second situation of interest is the *unipolar plasma*, where charges of only one polarity are dominant. This is strictly the case in SESI. In a corona discharge there is a small ionization region where ions of both polarities are formed from dissociation of neutral gas. However, the electric field is very intense, so the ions with polarity opposite to that of the emitting tip drift rapidly towards this tip, leaving in most of the gas only ions having the same polarity as the tip. The same would happen in ^{63}Ni or other bipolar sources in the presence of sufficiently strong electric fields. Once ions of a single polarity are left by themselves, their evolution will typically be dominated by the strong resulting space charge fields.

2.1. Neutral plasma

The equilibrium limit in this case is well known, but it is appropriate to summarize the results to facilitate the subsequent discussion. Let n_s, and n_v be the concentrations of ionized vapor molecules and neutral vapor. Let n_i be the concentration of charging ions, taken to be the same for the positive and negative polarities. If we ignore spatial variations, n_s is generated at a rate kn_vn_i due to ionization of the vapor by charge transfer from positive ions, and is destroyed at a rate $k_rn_sn_i$ due to recombination with negative ions:

$$\frac{dn_s}{dt} = kn_vn_i - k_rn_in_s. \tag{1}$$

In equilibrium, the two terms in the right hand side of (1) cancel exactly, leading to a fixed n_s/n_v ratio (2) independent of n_i. When this ratio is small it may be readily interpreted as the equilibrium charging probability:

$$p_{en} = \left(\frac{n_s}{n_v}\right)_{eq} = \frac{k}{k_r}. \tag{2}$$

The subscript n in p_{en} denotes that the charging plasma is neutral. The time scale to reach the steady state can be determined by examining the spatially uniform time dependent problem for (1) complemented by the corresponding Eq. (3) for ion production:

$$\frac{dn_i}{dt} = B - k_{ir}n_i^2. \tag{3}$$

Here B is the rate of ion formation per unit time and volume ($\mathrm{cm^{-3}\,s^{-1}}$), which depends on the intensity of the radioactive (or other bipolar) ion source. k_{ir} is the recombination rate corresponding to the charging ions, which may differ slightly from k_r. Depletion of charging ions by charge transfer to the vapor is ignored, so that the analysis is restricted to conditions where the vapor is present only in trace quantities. The equilibrium ion concentration n_{ie} is reached in a time of the order of τ according to (4) and (5), which once introduced in (1) yields (6)

$$\frac{n_i}{n_{ie}} = \tanh\left(\frac{t}{\tau}\right); \qquad n_{ie} = \left(\frac{B}{k_{ir}}\right)^{1/2} \tag{4}$$

$$\tau^{-1} = (Bk_{ir})^{1/2} = n_{ie}k_{ir} \tag{5}$$

$$\frac{n_s}{n_{se}} = 1 - \left[\cosh\left(\frac{t}{\tau}\right)\right]^{-k_r/k_{ir}}; \qquad n_{se} = \frac{n_vk}{k_r} \tag{6}$$

Fig. 1 plots the time dependent concentrations of charging ions and sample ions (at several values of the ratio k_r/k_{ir}), showing that both approach their equilibrium values within a few characteristic times τ. $1/\tau$ is linear with the concentration n_i of charging ions, showing that the smaller n_i, the harder it is to reach the equilibrium concentration.

Information on the values of these rate coefficients is important to quantify p_e, and some attention must necessarily be paid to it.

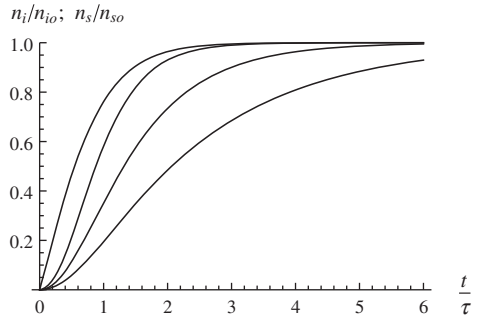

Fig. 1. Time dependence of the concentration of charging ions (left curve) and ionized vapor corresponding from left to right to k_r/k_{ir} values of 1/2, 1 and 2.

The rate k of vapor ionization is discussed in Appendix A. Its classical value k_p based on the ion-induced dipole (polarization) interaction is (Eq. (19) of [45])

$$k_p = \sqrt{\frac{\pi\alpha q^2}{\mu\varepsilon_o}} \tag{7a}$$

$$\mu = \frac{m_i m_v}{m_i + m_v}, \tag{7b}$$

where q is the charge of the ion, α is the polarizability of the vapor molecule and ε_o the electrical permittivity of vacuum. For a typical situation with vapors of the explosive PETN ionized by chloride, $\mu = 31.5$ Da, $\alpha \sim 20$ Å^3, $k \sim 2\times10^{-9}$ cm^{-3} s^{-1}. Various generalizations of Eq. (7a) are available. For instance, Gioumousis and Stevenson [45] account also for non-Boltzmann ion velocity distributions (irrelevant at atmospheric pressure, but important in interpreting mass spectrometric measurements of k). A permanent dipole in the vapor molecule may have a large effect [~fivefold in the calculations of [46] when the dipole is locked [47,48] during the collision period, as may be expected for light ions and heavy vapors. The effect is still substantial (~twofold in the calculations of [46]; Eq. (23) and Fig. 1) for a rapidly rotating permanent dipole].

The ion–ion recombination rate k_r is several orders of magnitude larger than k, as it is driven by the long range Coulomb attraction. In view of (2), this results in equilibrium ionization probabilities much smaller than unity. For instance, the approximate value $k_r \sim 10^{-6}$ cm^{-3} s^{-1} given at atmospheric pressure in [8] is ~1000 times k, leading to $p_e \sim 10^{-3}$. The recombination cross section for the strictly Coulombic interaction is zero for point particles because, at short distances, the centrifugal potential $(1/r^2)$ dominates over Coulomb's potential. However, once the finite size of the ions or other ion–ion interactions are retained (such as the attraction between one ion and a permanent or induced dipole in the other ion), the cross section becomes finite and very large compared to the geometrical cross section of the ion. Typical values calculated in Appendix B when accounting for the Coulombic and induced dipole interactions are $k_r \sim 10^{-7}$ cm^{-3} s^{-1}. These values apply at low enough pressures, where the process is dominated by two-body collisions [49]. The corresponding characteristic capture radius typically exceeds 6 nm, much larger than the geometrical radius of the ions. However, at ambient conditions, a sphere of that radius contains over 20 neutral molecules. Consequently a free-molecule analysis of the collision is inappropriate because the typically high velocity achieved (in vacuo) at the turning point of the Coulombically attracting ions is in reality moderated by collisions with the background. This leads to an increase of k_r with pressure [49]. There is consequently an undesirable decrease in ionization probability associated to an increase in k_r from about 10^{-7} cm^{-3} s^{-1} at low pressure to about 10^{-6} cm^{-3} s^{-1} at ambient pressure. This pressure dependence is important when comparing API to other low pressure ionization techniques. At sufficiently high pressures there must be a limit to the increase in k_r because ions of opposite polarity do not follow at all Newton's equations. Instead, they fall into each other's Coulombic field in an increasingly resistive medium, at a speed proportional to the sum of their mobilities (inversely proportional to pressure). Recombination then takes place in a finite time that depends on the initial inter-ionic distance. If this distance is fixed as the radius of a sphere containing on the average one ion, one finds [50,51]:

$$k_r = \frac{e(Z_s + Z_i)}{\varepsilon_o} \tag{8}$$

$$p_{eb} = \frac{k\varepsilon_o}{e(Z_s + Z_i)}. \tag{9}$$

For a typical situation in ambient air, with $Z_s + Z_i = 3$ cm^2 V^{-1} s^{-1}, $k_r = 5.4\times10^{-6}$ cm^{-3} s^{-1}. This rate now decreases with increasing pressure, so that there must be an intermediate pressure at which k_r is a maximum and the equilibrium charging efficiency is a minimum.

2.2. Unipolar ion sources and space charge limited ionization rate

Due to the strong space charge electric fields involved, the steady state conservation equation for the concentration n_s of ionized vapor cannot in this case ignore the motion of the ions. For simplicity we assume that the charging ions are of a single species of positive polarity, have concentration n_i, net charge q, and create a space charge field E according to Poisson's Eq. (10). The vapor molecules, once ionized have electrical mobility Z_s and evolve according to the steady mass conservation Eq. (11):

$$\nabla\cdot\boldsymbol{E} = \frac{n_i q}{\varepsilon_o} \tag{10}$$

$$\nabla\cdot[n_s(Z_s\boldsymbol{E})] = k n_v n_i, \tag{11}$$

where the space charge due to n_s has been ignored in (10) compared to that due to n_i. After expanding its left hand side, (11) becomes:

$$Z_s\boldsymbol{E}\cdot\nabla n_s = k n_v n_i - \frac{Z_s n_s n_i q}{\varepsilon_o} = n_i\left(k n_v - \frac{Z_s n_s q}{\varepsilon_o}\right). \tag{12}$$

The effective source of ionized vapors in the right hand side contains the same positive contribution $k n_v n_i$ from charge exchange as in (1), and a new negative contribution $Z_s n_s n_i q/\varepsilon_o$ from space charge dilution. This space charge dilution term is mathematically equivalent to the recombination term in (3), and its balance with the production term leads to a similarly simple result for the equilibrium ionization probability:

$$p_e = \left(\frac{n_s}{n_v}\right)_{eq} = \frac{k\varepsilon_o}{qZ_s}. \tag{13}$$

It is surprising that a phenomenon apparently as complex as ionizing a vapor in an undefined flow field and with an undefined cloud of charged particles could result in a fixed charging probability. Accordingly an additional effort to consolidate (13) will be undertaken in Section 3. Even more surprising is that the result (13) for space-charge-limited ionization is almost identical to (9) for recombination-limited ionization at high pressure, except for the substitution of $Z_s + Z_i$ in lieu of Z_s. For the time being, however, we will use (13) with appropriate information on the values of k, q and Z_s to provide a theoretical estimate of the charging probability.

2.2.1. Ionization from small ions

Here we consider the first charging model proposed by Fenn and colleagues, involving "charge exchange or chemi-ionization interactions between gas phase molecules and charged species produced in the ES process". In this case k is to first approximation given by k_p, the pure polarization result (7), whence:

$$(p_e)_{\text{ions}} = \sqrt{\frac{\pi\alpha\varepsilon_o}{\mu Z_s^2}}. \tag{14}$$

Typical values of α from the literature are collected in Appendix C for several explosives. Corresponding p_e values for ionization with $^{35}Cl^-$ also shown there are in all cases a few times 10^{-4}. They may perhaps reach up to $\sim10^{-3}$ for large vapor molecules with permanent dipoles, but this ionization process is generally fairly inefficient.

A more transparent approximate expression for the ionization probability may be obtained by using the polarization limit for the mobility of the ionized vapor [52]:

$$Z_s = \frac{0.51089}{n_g}\sqrt{\frac{\varepsilon_0}{\alpha_v\mu_{vg}}} \tag{15}$$

where μ_{vg} is the effective mass for vapor-carrier gas collisions, and n_g is the number concentration of carrier gas molecules. Substituting now (7) into (6) gives

$$p_e = 2.841\, n_g \left(\frac{\alpha_g \alpha \mu_{vg}}{\mu}\right)^{1/2}. \tag{16}$$

For the cases of interest m_v is substantially higher than the masses m_i and m_g of the charging ion and of the carrier gas molecules. Accordingly, the group $\mu_{vg}/\mu = (1+m_v/m_i)/(1+m_v/m_g) \sim m_g/m_i$ will typically be of order unity. n_g is also relatively fixed ($2.5\times10^{19}\,\mathrm{cm}^{-3}$ under atmospheric conditions), whence the dominant term determining the charging probability is the polarizability α of the vapor molecule. In spite of the high polarizabilities of the explosives included in Table C1, the slow $\alpha^{1/2}$ dependence gives little hope of substantial increase in ionization probability for most species having measurable room temperature volatilities. Eq. (16) shows also that the use of more massive and more polarizable carrier gases such as CO_2 may provide another twofold increase of p_e with respect to the values achievable in air. Conversely, a more substantial disadvantage would result from ionizing in lighter and less polarizable gases such as He, a gas frequently used in GC work [29].

2.2.2. Ionization from small drops

Here we consider the second ionization model proposed by Fenn and colleagues, where, presumably, "... *the gas phase molecules were collected by ES droplets, then emitted as ions as the droplet evaporated just as if they had been solutes in the sprayed solution*." In this case, in the extreme limit when all vapor molecules captured by an ES drop are ionized, k is given by the rate of collisions between a drop of radius R and the vapor molecules:

$$k_d = R^2 \sqrt{\frac{8\pi k_B T}{m_g}}, \tag{17}$$

$$q_d \sim \frac{1}{2} q_R = 4\pi(\gamma\varepsilon_o R^3)^{1/2}. \tag{18}$$

Estimating the charge on electrospray drops as half of the Rayleigh limit (18) we find:

$$(p_e)_d = \sqrt{\frac{k_B T}{2\pi m_v}\frac{R\varepsilon_o}{\gamma Z_s^2}} \tag{19}$$

For typical values $m_v = 200$ Da, $T = 298$ K, $R = 10$ nm, $\gamma = 0.04$ N/m and $Z_s = 2\,\mathrm{cm}^2/\mathrm{V/s}$, one finds p_e values also of a few times 10^{-4}. In reality the rate constant (17) and the charging probability (19) would have to be multiplied by the probability of ionization of the vapor molecule in the drop via ordinary ESI, which is at most unity. Eq. (19) is therefore an upper limit.

In conclusion, the space-charge-limited vapor ionization process based on electrospray drops is at least as inefficient as that based on electrospray-generated ions. In view of this approximate numerical coincidence of both probabilities, distinguishing the two mechanisms may be difficult based on the measurement of ionization probabilities only. A certain level of distinction can nonetheless be achieved by other means. For instance, Fuerstenau et al. [4] have shown that an involatile analyte introduced in the electrospray region as an aerosol yields analyte ions. In this case it is clear that ionization proceeds through the drops. Other efforts at distinguishing between these two mechanisms have been pursued [41,42,29,27], though without definitive conclusions. Other approaches could be tried based on the different parametric dependences of k_d [Eq. (19)] and k_p [Eq. (17)]. For instance, Eq. (19) shows that p_e increases with the size of the electrospray drops, which may be controlled to a certain extent. There are other important control factors that remain to be explored. For instance, direct charging from drops requires that the analyte vapor reaches the drop surface. However, this process is inhibited by the outward flow of evaporated drop material (the so called Stephan flow, important in drop combustion). Both this process and the time required for substantial drop evaporation (and conversion of the initial charging drop into charging ES ions) depend on the initial drop size and on the volatility of the solvent. Other complexities do enter into the picture. For instance, we have observed efficient SESI of large trialkyl amine vapors in an aqueous electrospray cloud, even for water-insoluble amines. This observation precludes a scenario where the vapor first dissolves in the drop and is then ionized; but it does not necessarily precludes an active role of the drop surface in ionizing the amine. A useful prediction from this analysis is that $p_e \sim 1/Z_s$, so that the ionization probability is directly proportional to the pressure in the ionization chamber (both for ion and for drop charging).

3. Relevance of p_e

We now return to the question of how representative of the real ionization probability is the equilibrium limit p_e just obtained. Note that Eq. (11) is a first order partial differential equation that may be written in the form (20) as an ordinary differential equation along the ion trajectories or characteristic lines (21), in terms of the relaxation time τ (22) and the equilibrium concentration for the ionized vapor $n_{s\text{-}eq}$ (23). t is the time elapsed as the ion moves along its trajectory:

$$\frac{dn_s}{dt} = -\frac{n_s - n_{seq}}{\tau}, \tag{20}$$

$$\frac{d\boldsymbol{x}}{dt} = Z_s \boldsymbol{E}, \tag{21}$$

$$\tau = \frac{\varepsilon_o}{n_i Z_s q}, \tag{22}$$

$$n_{s\text{-}eq} = p_e n_v. \tag{23}$$

This evolution equation for n_s has the typical form of a relaxation equation, with the simplifying feature that n_v (hence $n_{s\text{-}eq}$) is almost uniform in space and constant in time (simply because vapor is hardly consumed as a result of the tiny ionization probability). n_s therefore approaches $n_{s\text{-}eq}$ exponentially in time from an initial value (generally zero before mixing with the electrospray cloud). The time τ is the usual relaxation time for space charge dilution, which is inversely proportional to the charge density $n_i q$ of charging agents. Hence, for a point source where n_i diverges initially, τ is initially much smaller than any characteristic time in the problem, so that the equilibrium limit is achieved almost instantly. This advantage is peculiar of an ES source. For other initially less concentrated sources of ions or charged drops, the relaxation time may be larger than the residence time in the charger, leading to charging probabilities smaller than p_e.

4. Efficiency of SESI compared to other API and low pressure approaches

It is still too early to make a hard comparison between the various methods available for volatile ionization. Our own work with SESI has demonstrated outstanding detection levels [32–35], but has not included comparison with corona or radioactive sources. Hence, the fact that the latter two sources have not yet achieved the few ppq levels attained by SESI may simply relate to the fact that corona and ^{63}Ni sources remain to be tested in earnest with high sensitivity API mass spectrometers. The following comparison will therefore be based on theory and a few isolated observations, and should be considered provisional.

4.1. The role of pressure

It would seem at first sight that API sources are far more sensitive than those ionizing at reduced pressure. However, analytical instruments based on the latter have tended to use much smaller sample flow rates, so the comparison should be corrected for this drastic difference. Suppose a given flow rate of sample gas carrying neutral vapor is drawn into a low pressure system and ionized in the pressure range between 1 and 10 Torr. Ion guides are here far more effective in separating the gas from the ions than at atmospheric pressure, so the change would be beneficial in this respect. A bipolar ion source would also have improved performance since k_r would be typically reduced tenfold. However, the range of the α or β particles would be meters rather than cm. Alternatively, the radioactive source could be held at atmospheric pressure and the resulting bipolar plasma quickly sampled into a low pressure region where a higher equilibrium vapor ionization probability would still result from the reduced value of k_r. However, it would be difficult to achieve equilibrium because of the increased value of τ and the reduced residence time. Let us therefore shift our attention to unipolar sources. Because k is independent of pressure P (for both drop and ion charging), an interesting consequence of Eq. (13) is that the space-charge-limited ionization probability increases linearly with pressure P (since $1/Z \sim P$), suggesting that the higher the pressure the higher p_e. This is easily understandable since the space charge dispersion velocity is proportional to Z_s, so the smaller the mobility the less the dispersion. It is tempting to conclude generally that atmospheric pressure ionization methods would be more favorable than a diversity of other existing vapor ionization approaches taking place at reduced pressure, where polar vapor species are charged by proton transfer reactions (PTR) in a glow discharge [53–56]. The generalization would be correct as long as the charging ions are primarily of a single polarity (unipolar plasma). Nonetheless, the richness and variety of glow discharges (including neutral regions) needs to be considered in detail before coming to the final conclusion that the higher the pressure the better. Pending such a more careful investigation of glow discharge ionization, we are provisionally inclined to think that API is preferable. Subsequent discussion will therefore be confined to atmospheric ionizers. Note also that ES sources are difficult to stabilize between 100 Torr and 0.02 Torr [57,58].

4.2. SESI vs. corona discharge

We have argued that an ES source approaches closely the ideal of a point source of unipolar charge. The advantage of this situation is that equilibrium conditions are achieved instantly at the apex of the cloud of charged particles emerging from the tip of the Taylor cone. Consequently, the actual ionization probability is given by the equilibrium value p_e. In reality, if the charging mechanism were based on ions, because it takes a finite time for drop evaporation and ion release, the ideal situation imagined will not be met perfectly. A corona source is similar to a SESI source in this respect, since the bipolar ion production region has a small but finite volume, so a small departure from equilibrium would be expected. In either case, unipolar regions of very high ion concentrations are to be expected in the source region of both SESI and corona ionizers, whereby it is reasonable to assume that both will achieve equilibrium concentrations for the ionized vapor. The one direct comparison between SESI and corona charging available [43] may be insufficient to fully test this point. Nonetheless, the fact that both sources gave similar sensitivities for vapors [43] provides some level of confidence on the expectation that both sources are generally comparable. The fact that measured ionization probabilities for SESI [34,35] are comparable to the equilibrium value derived here provides further confirmation on the notion that both achieve space-charge-limited equilibrium ionization. This being so, the possible advantages of one source over the other must be associated to the peculiar details of their operation. The ES source is clearly superior from the point of view of not involving any superthermal phenomenon that might lead to decomposition of species. In particular, when analyzing a medium (such as the atmosphere) containing many organic vapors, some at high concentrations, there is good assurance that no greater complexity will be generated by decomposition of the original vapors. The same cannot be taken for granted in a corona discharge, where the fraction of the vapor sample contained in the small ion production region will yield undesired molecular fragments and reactive species. Conversely, although the SESI source does not create spurious species from gas phase components, unlike a corona, it injects impurity ions from the liquid. Also, solvent boiling sets limits to the gas temperature achievable in the SESI region. This difficulty has been overcome by Hill and colleagues via a water-cooled source, and is absent from corona sources. The boiling problem is nontrivial in many vapor analysis situations (particularly those involving GC), where relatively high temperatures are desirable to avoid vapor condensation or adsorption on surfaces. An interesting advantage of SESI is its ability to ionize small particles of involatile materials contained in the gas [4,34], which would normally not be ionized in a corona. Finally, a potential advantage of a corona is its expected higher dynamic range when analyzing concentrated vapors, following from its ability to produce higher ion currents than ESI. This point has not yet been demonstrated in practice for SESI, but it follows by analogy with the early studies of Carroll et al. [9]. When comparing a corona to a ^{63}Ni source, these authors found similar LDLs for both, but the dynamic range of the corona was superior. This advantage is evidently due to the delayed depletion of charging ions by charge transfer to the analyte when it is present at high concentrations. This dilution is not included in our analysis, which is therefore limited to highly diluted vapors. Another advantage of SESI is its great versatility for introduction nonvolatile reagent species.

4.3. SESI and corona discharge vs. radioactive sources

Based on strictly theoretical considerations, we have already noted that the upper limit for k_r yields a p_e value (8) similar to that theoretically applying to space charge-limited ionization. Because the actual k_r is smaller than this upper limit, the equilibrium ionization probability is likely to be higher for bipolar than unipolar chargers. On the other hand, the typical ion currents and concentrations achievable in bipolar ion sources are much smaller than in SESI or corona sources. Consequently, the actual ionization probability in ^{63}Ni sources will often tend to be less than the equilibrium value. This kinetic consideration would then explain why the few comparisons available between radioactive and SESI or corona source report either a comparable LDL [8] or an order of magnitude disadvantage for the ^{63}Ni source [43]. This situation is particularly clear in the studies of Tam and Hill [42] with RDX, where the peak intensity for the charging ions was comparable to that of the analyte.

5. Conclusions

When implemented in modern high-performance mass spectrometers, but otherwise very much as introduced by Fenn and colleagues, SESI-API-MS has demonstrated a remarkable sensitivity for vapor species in the atmosphere, with LDLs of a few ppq. Surprisingly, however, the corresponding literature (see [59,60] besides the publications discussed here) is growing slowly, and the outstanding merits of the approach are still insufficiently appreciated. This paper has attempted a comparison between SESI and a vari-

ety of other vapor ionizers. In view of the limited experimental information on the ionization probability p, we have determined its theoretical equilibrium value p_e for space-charge-dominated conditions. We also argue that, for point sources such as SESI and coronas, p approaches p_e. The few approximate experimental data available imply that $p \sim 10^{-4}$. This is comparable to p_e, confirming the usefulness of this theoretical limit, and enabling a discussion on the probable relative merits of various vapor ionization schemes. On this basis we have analyzed the role of pressure, concluding provisionally that atmospheric pressure sources are probably preferable to low pressure sources, while even super-atmospheric operation would be preferable in space-charge-limited situations. Both corona and SESI ionizers appear to have identical charging probabilities, both being close to the equilibrium value. Each has its own anticipated advantages and limitations in terms of total ion current, induced chemical noise, reagent introduction and temperature of operation. While p_e may in principle be better for radioactive than space-charge-limited sources, equilibrium is harder to reach in the former due to the generally smaller currents and ion concentrations attainable. These theoretical comparisons are in qualitative agreement with the few experimental data available, suggesting that perhaps the singular sensitivity positively demonstrated already for SESI sources might be applicable also to other situations.

Acknowledgments

It is a pleasure to thank John Fenn for the unique privilege of many years enjoying his advice and inspiration, for his generously given time and friendship, and for always providing exemplary standards of intellectual and personal integrity. I am grateful to my brother Gonzalo, and to his SEADM colleagues Pablo Martinez-Lozano, Juan Rus, Guillermo Vidal, Ana Pereira, Erica Mesonero and Alejandro Casado, for their many outstanding contributions to the development of SESI-API-MS. I thank Bruce Thomson of Sciex for his insights in the fields of atmospheric pressure ionization and mass spectrometry.

Appendix A. Charge exchange rate

A.1. Binary collision problem

Consider the collision of two point particles of masses m_1, m_2, and positions $\boldsymbol{r}_1$, $\boldsymbol{r}_2$, interacting with a central force field $\boldsymbol{F} = F(r)\boldsymbol{e}_r$ along the direction of their centers, where:

$$\boldsymbol{e}_r = \frac{\boldsymbol{r}}{r}, \quad r = |\boldsymbol{r}|, \quad \text{and} \quad \boldsymbol{r} = \boldsymbol{r}_1 - \boldsymbol{r}_2. \tag{A1}$$

Denoting by primes the time derivatives: $y' = dy/dt$, the equations of motion are

$$m_1 \boldsymbol{r}_1'' = F(r)\boldsymbol{e}_r \tag{A2a}$$

$$m_2 \boldsymbol{r}_2'' = -F(r)\boldsymbol{e}_r, \tag{A2b}$$

from which follows the first integral $m_1\boldsymbol{r}_1' + m_2\boldsymbol{r}_2' = Const$. Choosing the coordinate system moving with the center of mass, $Const = 0$ and $m_1\boldsymbol{r}_1 + m_2\boldsymbol{r}_2 = 0$. Combining this result with (A1) we may write

$$\boldsymbol{r}_1 = \frac{\boldsymbol{r}}{1 + m_1/m_2}; \qquad \boldsymbol{r}_2 = -\frac{\boldsymbol{r}}{1 + m_2/m_1}. \tag{A3}$$

(A2) may then be written in terms of $\boldsymbol{r}$ only:

$$\mu \boldsymbol{r}'' = F(r)\boldsymbol{e}_r; \quad \mu = \frac{m_1 m_2}{m_1 + m_2}. \tag{A4}$$

In polar coordinates r, θ, this vector equation yields the two scalar equations:

$$r'' = \frac{F(r)}{\mu} + r\theta'^2; \qquad r^2\theta' = C \tag{A5}$$

The energy Eq. (A6) follows from (A5) after elimination of θ' in terms of r and a first integration:

$$\frac{r'^2}{2} + \frac{C^2}{2r^2} + \frac{V(r)}{\mu} = \xi, \tag{A6}$$

where ξ is a constant, and the potential energy $V(r)$ is associated to the force via $F(r) = -dV(r)/dr$.

A.2. Polarization interaction

In the particular case of the polarization force associated to the interaction between an ion and the dipole it induces in the neutral vapor molecule with which it is about to exchange its charge, the potential energy for a singly charged ion takes the form[2]:

$$V(r) = -\frac{\alpha e^2}{8\pi\varepsilon_o r^4}. \tag{A7}$$

In the far field (large r), the repulsive centrifugal force dominates, while, at small r, the attractive force dominates. Therefore, particles with sufficient energy to overcome the centrifugal barrier will be trapped. For these, one assumes that there is 100% probability of charge exchange, as long as this is thermodynamically favorable. This is typically the case when the charge resides initially in a small ion and is to be transferred into a much larger polar neutral molecule. If one now considers a situation where the far field velocity of the particle with mass m_1 in the center-of-mass reference system is u_∞, and $C = bu_\infty$, then $\xi = u_\infty^2/2$. At the turning point $r = r_o$, $r' = 0$, hence

$$\frac{b^2 u_\infty^2}{2r_o^2} - \frac{\alpha e^2}{8\pi\mu\varepsilon_o r_o^4} = \frac{u_\infty^2}{2}. \tag{A8}$$

Dividing both sides by $u_\infty^2/2$ and introducing the notation

$$\beta = \frac{\alpha e^2}{4\pi\varepsilon_o \mu b^4 u_\infty^2}, \tag{A9}$$

(A8) takes the form (A10) with roots (turning points) given in (A11):

$$1 - \left(\frac{b}{r_o}\right)^2 + \beta\left(\frac{b}{r_o}\right)^4 = 0. \tag{A10}$$

$$\left(\frac{b}{r_o}\right)^2 = \frac{1 \pm (1 - 4\beta)^{1/2}}{2\beta} \tag{A11}$$

Since the outer turning point corresponds to the condition when the particle bounces, trapping corresponds to cases with no turning point, when $\beta > 1/4$. Hence,

$$\text{trapping arises when}: \quad b^4 u_\infty^2 < \frac{\alpha e^2}{\pi\varepsilon_o \mu} \tag{A12}$$

A.3. Charge exchange rate k

Trapping brings the neutal and the ion close enough to almost automatically lead to charge transfer in cases where this transfer is thermodynamically favored (energetically downhill). In such cases, the trapping and the charge transfer rates can be identified. For

[2] Indeed, if the dipole induced by a field $\boldsymbol{E}$ is $\boldsymbol{p} = a\boldsymbol{E}$, then the corresponding force is $\boldsymbol{F} = e\{\boldsymbol{E}(\boldsymbol{r} + \boldsymbol{d}) - \boldsymbol{E}(\boldsymbol{r})\} \sim e\boldsymbol{d}\cdot\nabla\boldsymbol{E} = \boldsymbol{p}\cdot\nabla\boldsymbol{E} = a\boldsymbol{E}\cdot\nabla\boldsymbol{E} = a\nabla E^2/2$. We follow the usual approach of defining the polarizability $\alpha = a/(4\pi\varepsilon_o)$ such that α has units of volume. When $\boldsymbol{E}$ is Coulomb's field $e/(4\pi\varepsilon_o r^2)$, then one obtains the potential energy (A7).

simplicity we consider the limit when the neutral molecule is much heavier than the ion, so that the neutral is at rest at the center or mass, and the ion has a Maxwellian velocity distribution function

$$f(\boldsymbol{u}) = n_i\left(\frac{2\pi k_B T}{m_i}\right)^{-3/2} \exp\left[\frac{-m_i u^2}{2k_B T}\right].$$

A generalization of this approximation to arbitrary mass ratios can be obtained by a double integration of the two velocity distribution functions over their respective velocity variables. The difference between the exact and the approximate result is that m_i rather than μ appears, so, the substitution $m_i \to \mu$ will be made at the end of the calculation without further comment.

The collision frequency with a given vapor molecule is

$$kn_i = \int_0^\infty 2\pi b db \iiint |\mathbf{u}| f(\mathbf{u}) d^3\mathbf{u}, \tag{A13a}$$

where the velocity integration is in the domain (A12). Exploiting the spherical symmetry of the velocity integral and introducing the variables x and y, we may write

$$k = \pi^{-3/2}\sqrt{\frac{2k_B T}{m_i}} \int_0^\infty 2\pi b db \int_0^y 4\pi e^{-x^2} x^3 dx;$$

$$y^2 = \frac{m_i \alpha e^2}{2\pi\varepsilon_o \mu k_B T b^4}; \qquad x^2 = \frac{m_i u^2}{2k_B T}. \tag{A13b}$$

Shifting now from the b to the y variable introduced in (A13b), and noting that

$$\int_0^y e^{-x^2} x^3 dx = \frac{1-(1+y^2)e^{-y^2}}{2}, \quad \text{we find:}$$

$$k = 2A\sqrt{\frac{\alpha e^2}{\mu\varepsilon_o}}, \quad \text{with } A = \int_0^\infty \frac{dy}{y^2}[1-(1+y^2)e^{-y^2}] = \frac{\sqrt{\pi}}{2}. \tag{A13c}$$

This leads to the familiar result [45]:

$$k = \sqrt{\frac{\pi\alpha e^2}{\mu\varepsilon_o}}. \tag{A14}$$

For a typical situation with $\mu = 30$ Da, $\alpha = 20$ Å^3, $k = 1.9\times10^{-9}$ cm^3 s^{-1}.

A.4. Effect of the finite ion diameter on the ionization probability

Most of the explosive vapors used in the prior calculations have electrical mobilities clearly smaller than the polarization limit. Their cross sections and corresponding k are therefore larger than indicated by the polarization limit. Also, Z_s should be smaller than the 2 cm^2/V/s used to compute p_e approximately in Table C1. These two finite size effects will therefore increase the ionization probability with respect to the calculated values in Table C1. In order to account for this, we will assign a finite radius to these vapor molecules, and assume that there is charge exchange when the ion touches the vapor molecule. Denoting by ε the sum of the ion radius and the vapor molecule radius, capture will therefore take place when either $\beta > 1/4$ (as before, when there was no turning point), or when the turning point for the point particle problem is such that $r_o < \varepsilon$. In the limit $\varepsilon = 0$, the position of the outer turning point is given from (A11) as

$$\left(\frac{r_o}{b}\right)^2 = \frac{1+(1-4\beta)^{1/2}}{2}. \tag{A19}$$

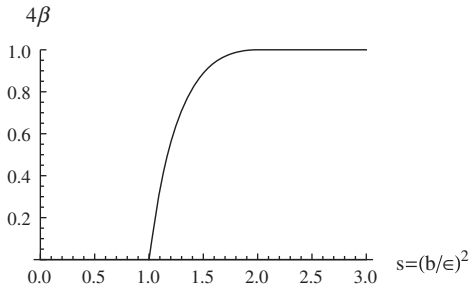

Fig. A1. Critical β.

r_o/b therefore lies always between 1/2 and 1. If $\varepsilon/b < 1/2$, then $r_o > \varepsilon$, there is no effect of the finite vapor radius, and things are as before (capture requires $\beta > 1/4$). However, in the interval $1/2 < \varepsilon/b < 1$, r_o and ε are in the same range of values, and they coincide for a certain value of $\beta < 1/4$. In this range the critical β for capture is less than 1/4, and is given by the condition $r_o(\beta) = \varepsilon$, namely:

$$\beta = \left(\frac{\varepsilon}{b}\right)^2 - \left(\frac{\varepsilon}{b}\right)^4; \qquad 1 < \frac{b}{\varepsilon} < 2 \tag{A20}$$

Finally, for $\varepsilon/b > 1$, r_o is always smaller than ε, so that capture takes place for any β. Capture conditions therefore take the form (A21), above the curve shown in Fig. A1, while scattering takes place below it

$$\beta > \beta^*(s); \qquad s = \left(\frac{b}{\varepsilon}\right)^2 \tag{A21a}$$

$$\beta^*(s) = 0, \quad \text{for } 0 < s < 1 \tag{A21b}$$

$$\beta^*(s) = s^{-1} - s^{-2}, \quad \text{for } 1 < s < 2 \tag{A21c}$$

$$\beta^*(s) = 1/4, \quad \text{for } s > 2. \tag{A21d}$$

k is obtained with an integration similar to (A13b), except that β^* is no longer $\sim b^{-4}$, but takes a more complex dependence on $s = (b/\varepsilon)^2$. We now write β in terms of the dimensionless quantities s and x and the dimensionless parameter λ rather than u, b:

$$2\beta^{1/2} = \frac{\lambda}{sx}; \qquad \lambda^2 = \frac{\alpha e^2}{2\pi\varepsilon_o k T \varepsilon^4},$$

whereby the condition $\beta > \beta^*(s)$ becomes $4s^2x^2 < \lambda^2/\beta^*(s)$. Using also the fact that

$$\int_0^y x^3 e^{-x^2} dx = \frac{1}{2}[1 - e^{-y^2}(1+y^2)],$$

$$\text{we find } \quad k = 2c\varepsilon^2 F(\lambda); \qquad c = \sqrt{\frac{8\pi k_B T}{\mu}} \tag{A22}$$

$$F(\lambda) = \int_0^\infty ds \int_\Gamma x^3 e^{-x^2} dx \tag{A23}$$

$$= \frac{1}{2}\int_0^\infty ds[1 - [1+z(s)]e^{-z(s)}], \tag{A24}$$

$$z(s) = \frac{\lambda^2}{4s^2\beta^*(s)}. \tag{A25}$$

The domain of integration Γ is the region $\beta > \beta^*(s)$, where $4s^2x^2 < \lambda^2/\beta^*(s)$.

Note that we have substituted the value m_i appearing in (A22) and (A25) by μ, since the simplified approach followed is valid only in the limit $m_v \gg m_i$.

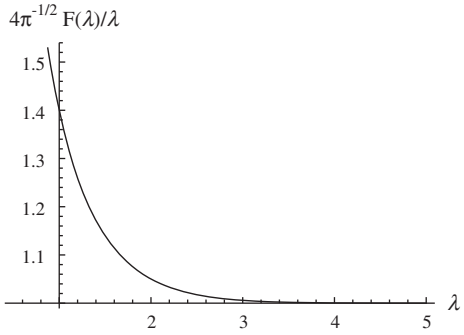

Fig. A2. Correction factor to the pure polarization limit (A14) for k associated to the finite radius ε of the vapor–ion pair.

In view of (A21), $F(\lambda)$ can be computed as

$$2F(\lambda) = \int_0^1 ds + \int_1^2 ds \left\{ 1 - \left(1 + \frac{\lambda^2/4}{s-1} \right) \exp\left[\frac{-\lambda^2/4}{s-1} \right] \right\} + \int_2^\infty ds \left[1 - \left[1 + \frac{\lambda^2}{s^2} \right] e^{-\lambda^2/s^2} \right]. \quad \text{(A26)}$$

The second and third integrals are $1-\exp[\lambda^2/4]$ and $-2(1-\exp[\lambda^2/4])+(1/2)\lambda\pi^{1/2}\,Erf[\lambda/2]$, whence

$$2F(\lambda) = e^{-\lambda^2/4} + \frac{\lambda\sqrt{\pi}}{2} Erf\left(\frac{\lambda}{2}\right), \quad \text{(A27)}$$

where Erf is the error function that tends to unity as $\lambda \to \infty$. The pure polarization limit (A14) corresponds to $F(\lambda) \to \lambda\sqrt{\pi}/4$, and finite size effects introduce the correction factor $4F(\lambda)/\lambda/\pi^{1/2}$ shown in Fig. A2. It is relatively close to unity (<1.05) for $\lambda > 2$. At $\lambda = 1$, it exceeds unity by a substantial 1.4 factor.

The radius of a typical explosive vapor is 0.5 nm, and that of the charging ion perhaps 0.2 nm. Therefore, typically, $\varepsilon = 0.7$ nm. For singly charged ions at room temperature, (A25) becomes:

$$\lambda = \lambda_o \alpha^{1/2} \varepsilon^2; \qquad \lambda_o = 33.75\,\text{Å}^{\,1/2}. \quad \text{(A28)}$$

Therefore, with $\alpha = 10$ Å^3 and $\varepsilon = 7$ Å, (A28) gives $\lambda = 2.18$, with a trivial correction factor of 1.1. In conclusion, although the explosive vapors of interest are unusually large, their polarizability is also large, leading to sufficiently large λ values for the pure polarization formula to be reasonably accurate.

The error associated to the use of the polarization limit (15) for the electrical mobility is not so trivial (because the corresponding α_v is an order of magnitude smaller than α). Typical Z_s values for explosives are 1 cm^2/V/s, while the polarization limit in air or N_2 is about twice as large. This may double the estimated charging probabilities reported in the last column of Table C1 (for N_2 gas at ambient conditions, based on (A18) with $\mu_{vg}/\mu = 1$). Therefore, the determination of the charging probability (A16) should be based on experimental values of Z_s, and either the polarization limit for k, or the slightly larger value following from (A22) and (A27). Estimated values for Z_s at room temperature are included in Appendix C.

Appendix B. The ion–ion recombination rate

The analysis will ignore ion-electron recombination. This is appropriate at pressures high enough for electrons to be rapidly captured by neutrals, but is not necessarily the case in glow discharges at lower pressure. The energy Eq. (A6) may be written for the Coulombic interaction between two singly charged particles:

$$\frac{r'^2}{u_\infty^2} + \frac{b^2}{r^2} - \frac{2\gamma}{r} = 1, \qquad \gamma = \frac{e^2}{4\pi\varepsilon_o \mu u_\infty^2 k_B T} \quad \text{(B1)}$$

let $r = r_o$ be the turning point where $r' = 0$:

$$r_o = -\gamma + (\gamma^2 + b^2)^{1/2}. \quad \text{(B2)}$$

There is always a turning point because, at close range, the centrifugal potential ($\sim r^{-2}$) always dominates over the Coulombic potential ($\sim r^{-1}$). Impact will therefore never take place for point particles, unless there is an additional close-range mechanism for capture. One possibility is to include polarization. Another is to include the finite size ε of the colliding ions, and suppose that thermodynamically allowed capture takes place if $r_o < \varepsilon$. We shall consider both limits.

B.1. Ions of finite size

The condition $r_o < \varepsilon$ for capture may be written

$$b^2 < \varepsilon^2 + \frac{e^2\varepsilon}{2\pi\varepsilon_o \mu u_\infty^2} \quad \text{(B3)}$$

whence the integral of bdb may be performed immediately turning (A13a) for k_r into

$$k_r = \varepsilon^2 c \int_0^\infty e^{-x} dx \left(x + \frac{\Lambda}{\varepsilon} \right) = c\varepsilon(\Lambda + \varepsilon), \quad \text{(B4a)}$$

where the thermal velocity c was defined in (A22), and we have introduced the characteristic length Λ ($\Lambda \sim 57$ nm for singly charged ions at room temperature):

$$\Lambda = \frac{e^2}{4\pi\varepsilon_o k_B T}. \quad \text{(B4b)}$$

The cross section includes two additive terms: one, $c\varepsilon^2$, corresponding exactly to that for a pure hard sphere without Coulombic attraction. The other is a Coulombic term linear in ε. The enhancement factor $1 + \Lambda/\varepsilon$ diverges as $1/\varepsilon$, but the cross section is finite even for $\varepsilon = 0$. Suppose $\varepsilon = 0.65$ nm. At room temperature the enhancement factor $1 + \Lambda/\varepsilon \sim 88.7$, and the effective capture radius is 6.6 nm. The resulting $k_r = 5.7 \times 10^{-8}$ cm^{-3} s^{-1} is two orders of magnitude larger than the value based on the geometric cross section, but still underestimates the actual recombination rate under atmospheric conditions. Because $\Lambda/\varepsilon \gg 1$, (B4a) is well approximated by:

$$k_r = c\varepsilon\Lambda, \quad (\Lambda \gg \varepsilon). \quad \text{(B4c)}$$

B.2. Polarizable ions

We will assume that the polarizability of the vapor ion is the same as that of the neutral vapor. In reality the net charge attached to the vapor molecule creates a permanent dipole, in addition to the dipole induced by the colliding ion. Although this permanent dipole is rotating, its average effect is not null, and has been considered by Su and Bowers [46]. The dipole induced by the small ion on the vapor is not rotating and is the only one considered here. In this case the Coulomb force pulls effectively the ions from far away, and when they are close enough and ready to bounce due to the centrifugal force, the short range polarization attraction captures them. There is hence no need to take into account ion size. Notice that each of the two colliders induces a dipole on its partner so that the effective α used in (B5) includes the two corresponding forces. The energy equation is:

$$\frac{r'^2}{u_\infty^2} + \frac{b^2}{r^2} - \frac{2\gamma}{r}\left(1 + \frac{\alpha}{2r^3}\right) = 1 \quad \text{(B5)}$$

Turning points correspond to $r' = 0$, $r = r_o$ in (B5), written as (B6) in terms of the dimensionless variables a and ξ defined in

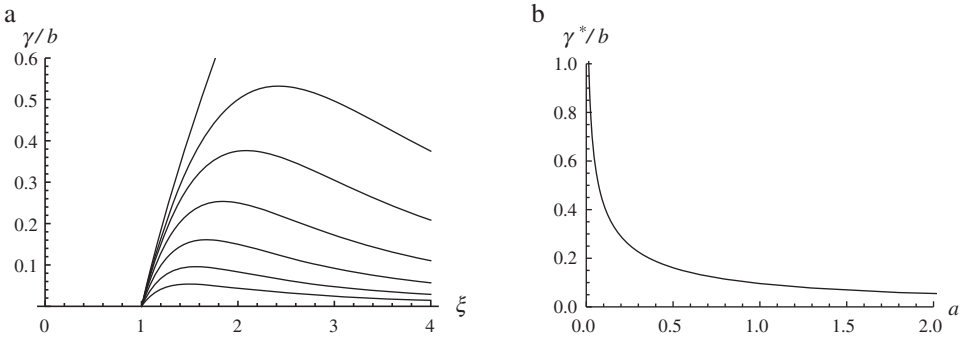

Fig. B1. Critical conditions for capture of oppositely charged ions accounting for the induced dipoles. Left: representation of (B6b) for $a=(1/2)\alpha/b^3=1/16, 1/8, 1/4, 1/2, 1, 2$, showing that no turning point exists for γ/b above a certain critical value γ^*/b. Right: dependence of γ^*/b on a.

(B7) and (B8)

$$\xi^2 - 2\xi\left(\frac{\gamma}{b}\right)(1+a\xi^3)=1, \tag{B6}$$

$$a=\frac{\alpha}{2b^3}, \tag{B7}$$

$$\xi=\frac{b}{r_o}. \tag{B8}$$

Rather than solving this quartic equation for ξ, it is simpler to solve for γ/b:

$$\frac{\gamma}{b}=\frac{\xi-1/\xi}{2(1+a\xi^3)}. \tag{B6b}$$

For $\alpha=0$, $\xi-1/\xi$ increases monotonically from $-\infty$ to $+\infty$. Accordingly, as seen in (B2), there is always a turning point for all γ. However, for all $\alpha>0$, the cubic term in the denominator of (B6b) introduces a maximum in $\gamma(\xi)$ (Fig. B1a). There are consequently two turning points for γ/b below a critical value γ^*/b, and none above it. This critical γ^*/b may be determined for each $a>0$ through the point with zero slope in the curves of Fig. B1a. The domain of capture is therefore

$$\Gamma:\ \frac{\gamma}{b}>\frac{\gamma^*}{b}=\Phi(a). \tag{B9a}$$

The critical curve (B9a) is shown in Fig. B1b. It may be computed from the condition that the derivative of (B6b) with respect to ξ be zero, which yields (B9b). Substituting this expression into (B6b) gives (B9c), providing a parametric representation of (B9a):

$$a=\frac{1+\xi^2}{2\xi^3(\xi^2-2)}, \tag{B9b}$$

$$\Phi=\frac{\xi^2-2}{3\xi}. \tag{B9c}$$

The function $a^*(\Phi)$ inverse to $\Phi(a)$ may be written explicitly by noting that (B9c) is a quadratic equation giving $\xi(\Phi)$, which substituted in (B9b) yields:

$$a*(\Phi)=\frac{8+4\Phi(3\Phi+\sqrt{8+9\Phi^2})}{\Phi(3\Phi+\sqrt{8+9\Phi^2})^4}. \tag{B10a}$$

k_r may now be computed as the integral (A13a) over the domain Γ defined in (B9a):

$$k_r=4c\iint_{\Gamma} e^{-x^2}x^3\,dx\,b\,db; \qquad x^2=\frac{\mu u_\infty^2}{2k_BT}. \tag{B10b}$$

If we now use the characteristic length Λ introduced in (B4b) and shift from the (x,b) variables into the new integration variables $\Phi=\gamma/b$ and a, we find

$$k_r=\frac{2\Lambda^2}{3}c\int_0^\infty\frac{d\Phi}{\Phi^3}\int_{a*(\Phi)}^\infty\frac{da}{a}\exp\left[\frac{-Ca^{1/3}}{\Phi}\right], \tag{B11}$$

$$C=\Lambda\left(\frac{2}{\alpha}\right)^{1/3}, \tag{B12}$$

The second of these two integrals is simply related to the incomplete Gamma function $\Gamma(n,x)=\int_x^\infty x^{n-1}e^{-x}dx$, leading finally to:

$$k_r=2\Lambda^2cG(C), \tag{B13}$$

$$G(C)=\int_0^\infty\frac{d\Phi}{\Phi^3}\Gamma\left(0,[a^*(\Phi)]^{1/3}\frac{C}{\Phi}\right). \tag{B14}$$

The integral G is convergent for all $C>0$, with computed values shown in Fig. B2. For singly charged particles at room temperature $\Lambda=57$ nm, while, for a typical polarizability $\alpha=20$ Å^3, $(\alpha/2)^{1/3}=0.215$ nm, resulting in a very large ratio $C=268$. As seen in Fig. B2b, $CG(C)$ is almost constant (from 1.89775 to 1.89067) in the realistic range $100<C<1000$. Hence, $CG(C)=1.891$ ($\pm0.37\%$) for

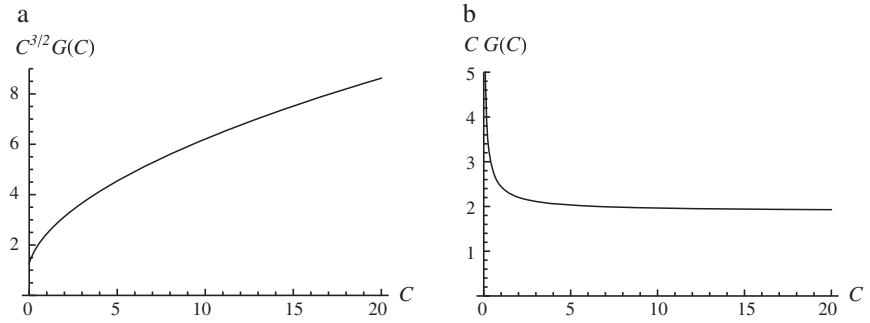

Fig. B2. Function $G(C)$ determining the recombination rate (B13) and (B14) of polarizable ions. Left: behavior at small C; right: behavior at large C.

Table C1
Polarizabilities α of explosive vapors, and predictions for k and p_e.

Vapor	α (Å^3)	α [63] (Å^3)	α [64][a] (Å^3)	m_v (Da)	$\mu_{v\text{-}Cl}$[b] (Da)	Ion	Z[c] (cm^2/V/s)	$10^9\,k$ cm^{-3} s^{-1}	$10^4\,p_e$[d]
EGDN	7.98 [61]	9.5	10.72	152.1	28.42	EGDN + Cl^-	1.63	1.35	3.66
PETN	16.3 [61]	20.19	22.49	316.14	31.51	PETN + Cl^-	1.30	1.87	5.13
TNT	15.6 [62]	18.25	19.9	227.13	30.33	$(TNT - H^+)^-$	1.65	1.82	5.01
RDX	12.3 [62]	15.47	17.35	222.12	30.24	RDX + Cl^-	1.51	1.67	4.56

[a] Calculations kindly provided by Dr. P. Martinez-Lozano, based on the SPARC database [64].
[b] The charging ion is $^{35}Cl^-$.
[c] Approximate electrical mobilities of the ions indicated in column 5, based on raw data kindly provided by A. Pereira and A. Casado (SEADM).
[d] From Eq. (6), with α from Bosque and Sales [63], and $Z_s = 2$ cm^2 V^{-1} s^{-1}.

$100 < C < 1000$, and (B13) reduces to

$$k_r \sim 3c\Lambda\alpha^{1/3}(\pm 0.37\%); \quad 100 < C < 1000. \tag{B15}$$

The expression is almost identical to (B5), except for the substitution of the geometric radius ε for the effective polarization radius $3\alpha^{1/3}$. At room temperature and with $\mu = 30$ Da, we find $k_r = 6.7 \times 10^{-8}$ cm^{-3} s^{-1}. The effective radius $(3\Lambda\alpha^{1/3})^{1/2}$ is 6.84 nm, slightly larger than the value obtained in the model with no polarization and finite ion size. These values are close to those measured for ions in the upper atmosphere, including the predicted temperature dependence $k_r \sim T^{-0.5}$ ($T^{-0.4}$ measured by Smith and Church [49]). As noted in the body of the article, at high pressures, the rate is dominated by three body collisions and is substantially larger.

Appendix C. Typical space-charge-limited ionization probabilities

Table C1 includes estimates for various parameters determining charge exchange rates and equilibrium ionization probabilities of four explosive vapors. Columns 2–4 show polarizabilities for the vapor species. Column 2 is from several published sources. Column 3 is based on the method of [63] (claimed to be more accurate than other calculations), giving the molecular polarizability as a linear combination of the atomic polarizabilities of the constituents of the molecule. k is from (A14). Column 4 was provided by Dr. P. Martinez Lozano based on the SPARC database [64]. The agreement between these various determinations of α provides a good level of confidence. p_e is based on Eq. (14), α from [63], and $Z_s = 2$ cm^2 V^{-1} s^{-1} (close to the polarization limit). The column Z shown in the table is based on relative measurements by A. Pereira and A. Casado (SEADM), and provides an indication of the error introduced in p_e by the assumption $Z_s = 2$ cm^2 V^{-1} s^{-1}. We turn these relative data into approximate mobilities via an absolute mobility scale determined by extrapolating the mass dependence of $Z_o = Z/(1 + m_g/m_v)^{1}/^{2}$ to zero mass, and assigning to this asymptote the polarization limit in N_2: $Z_o = 2.13$ cm^2 V^{-1} s^{-1} ($m_g = 28$ Da).

References

[1] D.R. Herschbach, Molecular Dynamics of Elementary Chemical Reactions; From Nobel Lectures, Chemistry 1981–1990, Chemistry 1986, Editor-in-Charge Tore Frängsmyr, Editor Bo G. Malmström, World Scientific Publishing Co., Singapore, 1992, pp. 265–314.
[2] V.H. Reis, J.B. Fenn, Separation of gas mixtures in supersonic jets, J. Chem. Phys. 39 (1963) 3240–3250;
Also V.H. Reis, Ph.D. thesis, Princeton University (1962).
[3] J. Fernández de la Mora, The heavy molecule-aerosol analogy, and the dispersion of sound by gas mixtures of disparate masses, J. Phys. Chem. 88 (1984) 4557–4560.
[4] S. Fuerstenau, P. Kiselev, J.B. Fenn, ESIMS in the analysis of trace species in gases, in: Proceedings of the 47th ASMS Conference on Mass Spectrometry Allied Topics, June 1999, Dallas, TX, 1999, ThOE 3:00.
[5] C.M. Whitehouse, F. Levin, C.K. Meng, J.B. Fenn, Proceeding of the 34th ASMS Conference on Mass Spectrometry and Allied Topics, June 8–13, 1986, Cincinnati, OH, 1986, p. 507.
[6] P. Kiselev, J.B. Fenn, ESIMS analysis of vapors at trace levels, in: Proceedings of the 49th ASMS Conference on Mass Spectrometry and Allied Topics, May 27–31, 2001, Chicago, IL, 2001.
[7] C. Wu, W.F. Siems, H.H. Hill, Proceedings of the 46th ASMS Conference on Mass Spectrometry and Allied Topics, Orlando, June 1998, 1998.
[8] E.C. Horning, M.G. Horning, D.I. Carroll, I. Dzidic, R.N. Stillwell, New picogram detection system based on a mass spectrometer with an external ionization source at atmospheric pressure, Anal. Chem. 45 (6) (1973) 936–943.
[9] D.I. Carroll, I. Dzidic, R.N. Stillwell, K.D. Haegele, E.C. Horning, Atmospheric pressure ionization mass spectrometry: corona discharge ion source for use in liquid chromatograph–mass spectrometer-computer analytical system, Anal. Chem. 47 (14) (1975) 2369–2373.
[10] R.K. Mitchum, W.A. Korfmacher, G.F. Moler, D.L. Stalling, Capillary gas chromatography/atmospheric pressure negative chemical ionization mass spectrometry of the 22 isomeric tetrachlorodibenzo-p-dioxins, Anal. Chem. 54 (4) (1982) 720–722.
[11] J.B. Fenn, Mass spectrometric implications of high-pressure ion sources, Int. J. Mass Spectrom. 200 (2000) 459–478.
[12] J.A. Buckley, J.B. French, N. Reid, Can. Aeronaut. Space J. 20 (1974) 231.
[13] J.B. French, N.M. Reid, J.A. Buckley, Method and apparatus for analyzing trace components using a gas curtain, US Patent 4,137,750 (1979).
[14] B.A. Thomson, J.V. Iribarne, Field induced ion evaporation from liquid surfaces at atmospheric pressure, J. Chem. Phys. 71 (11) (1979) 4451–4463;
(b) B.A. Thomson, J.V. Iribarne, The fate of electrical charges in evaporating cloud droplets, Rev. Geophys. Space Phys. 16 (3) (1978) 431–434;
B.A. Thomson, J.V. Iribarne, P.J. Dziedzic, Liquid ion evaporation/mass spectrometry/mass spectrometry for the detection of polar and labile molecules, Anal. Chem. 54 (1982) 2219–2224.
[15] D.A. Lane, B.A. Thomson, Monitoring a chlorine spill from a train derailment, J. Air Pollut. Control Assoc. 31 (2) (1981) 122–127.
[16] M. Yamashita, J.B. Fenn, Electrospray ion source, another variation of the free-jet theme, J. Phys. Chem. 88 (20) (1984) 4459–4465.
[17] M. Yamashita, J.B. Fenn, Negative ion production with the electrspray ion source, J. Phys. Chem. 88 (1984) 4671–4675.
[18] C.K. Meng, M. Mann, J.B. Fenn, Of protons and proteins, Z. Phys. D 10 (1988) 361–368.
[19] J.B. Fenn, M. Mann, C.K. Meng, S.K. Wong, C. Whitehouse, Electrospray ionization for mass spectrometry of large biomolecules, Science 246 (1989) 64–71.
[20] J.B. Fenn, M. Mann, C.K. Meng, S.K. Wong, C. Whitehouse, Electrospray ionization, principles and practice, Mass Spectrom. Rev. 9 (1990) 37–79.
[21] M.L. Vestal, High-performance liquid chromatography–mass spectrometry, Science 226 (4672) (1984) 275–281.
[22] D.J. Douglas, Linear quadrupoles in mass spectrometry, Mass Spectrom. Rev. 28 (2009) 9377–9960.
[23] A. El-Faramawy, K.W.M. Siu, B.A. Thomson, Efficiency of nano-electrospray ionization, J. Am. Soc. Mass Spectrom. 16 (10) (2005) 1702–1707.
[24] H. Javaheri, B.A. Thomson, Proceedings of the 57th ASMS Conference on Mass Spectrometry and Allied Topics, June 2007, Indianapolis, IN, 2007.
[25] T.R. Covey, B.A. Thomson, B.B. Schneider, Atmospheric pressure ion sources, Mass Spectrom. Rev. 28 (2009) 870–897.
[26] C.M. Whitehouse, R.N. Dreyer, M. Yamashita, J.B. Fenn, Electrospray interface for liquid chromatographs and mass spectrometers, Anal. Chem. 57 (3) (1985) 675–879.
[27] C.Y. Lee, J. Shiea, Gas chromatography connected to multiple channel electrospray ionization mass spectrometry for the detection of volatile organic compounds, Anal. Chem. 70 (13) (1998) 2757–2761.
[28] C.N. McEwen, R.G. McKay, A combination atmospheric pressure LC/MS:GC/MS ion source: advantages of dual AP-LC/MS:GC/MS instrumentation, J. Am. Soc. Mass Spectrom. 16 (2005) 1730–1738.
[29] N. Brenner, M. Haapala, K. Vuorensola, R. Kostiainen, Simple coupling of gas chromatography to electrospray ionization mass spectrometry, Anal. Chem. 80 (21) (2008) 8334–8339.
[30] M. Ishimaru, M. Yamada, I. Nakagawa, S. Sugano, Analysis of volatile metabolites from cultured bacteria by gas chromatography/atmospheric pressure chemical ionization-mass spectrometry, J. Breath Res. 2 (2008) 037021.
[31] A. Carrasco-Pancorbo, E. Nevedomskaya, T. Arthen-Engeland, T. Zey, G. Zurek, C. Baessmann, A.M. Deelder, O.A. Mayboroda, Gas chromatography/atmospheric pressure chemical ionization-time of flight mass spectrometry: analytical validation and applicability to metabolic profiling, Anal. Chem. 81 (2009) 10071–10079.
[32] P. Martinez-Lozano, J. Fernández de la Mora, Detection of fatty acid vapors in human breath by atmospheric pressure ionization mass spectrometry, Anal. Chem. 80 (21) (2008) 8210–8215.

[33] P. Martinez-Lozano, J. Fernández de la Mora, Direct mass spectrometric analysis of human skin vapors charged by secondary electrospray ionization, J. Am. Soc. Mass Spectrom. 20 (2009) 1060–1063.
[34] P. Martinez-Lozano, J. Rus, G. Fernández de la Mora, M. Hernández, J. Fernández de la Mora, Secondary electrospray ionization (SESI) of ambient vapors for explosive detection at concentrations below parts per trillion, J. Am. Soc. Mass Spectrom. 20 (2009) 287–294.
[35] E. Mesonero, J.A. Sillero, M. Hernández, J. Fernandez de la Mora, Secondary electrospray ionization (SESI) detection of explosive vapors below 0.02 ppt on a Triple quadrupole with an atmospheric pressure source, in: Poster Presented at the ASMS Annual Conference, May 31–June 4, 2009, Philadelphia, PA, 2009, http://www.seadm.com/descargas/Poster_Api%205000_09_EMS%203.pdf.
[36] R.W. Purves, R. Guevremont, S. Day, C.W. Pipich, M.S. Matyjaszczyk, Mass spectrometric characterization of a high-field asymmetric waveform ion mobility spectrometer, Rev. Sci. Instrum. 69 (1998) 4094–4104.
[37] A.A. Shvartsburg, K. Tang, R.D. Smith, FAIMS operation for realistic gas flow profile and asymmetric waveforms including electronic noise and ripple, J. Am. Soc. Mass Spectrom. 16 (2005) 1447–1455.
[38] B.B. Schneider, T.R. Covey, S.L. Coy, E.V. Krylov, E.G. Nazarov, Chemical effects in the separation process of a differential mobility/mass spectrometer system, Anal. Chem. 82 (2010) 1867–1880.
[39] J. Fernández de la Mora, L. de Juan, T. Eichler, J. Rosell, Differential mobility analysis of molecular ions and nanometer particles, Trends Anal. Chem. 17 (1998) 328–339;
H. Javaheri, Y. Le Blanc, B.A. Thomson, J. Fernandez de la Mora, J. Rus, J.A. Sillero-Sepúlveda, Analytical characteristic of a differential mobility analyzer coupled to a triple quadrupole system (DMA-MSMS), poster 061, in: Annual ASMS Conference, 1–6 June, 2008, Denver, Colorado, 2008.
[40] Y.H. Chen, H.H. Hill Jr., J. Microcolumn Sep. 6 (1994) 515–524.
[41] C. Wu, W.F. Siems, H.H. Hill Jr., Secondary electrospray ionization ion mobility spectrometry/mass spectrometry of illicit drugs, Anal. Chem. 72 (2000) 396–403.
[42] M. Tam, H.H. Hill Jr., Secondary electrospray ionization-ion mobility spectrometry for explosive vapor detection, Anal. Chem. 76 (10) (2004) 2741–2747.
[43] W.E. Steiner, B.H. Clowers, P.E. Haigh, H.H. Hill, Secondary ionization of chemical warfare agent simulants: atmospheric pressure ion mobility time-of-flight mass spectrometry, Anal. Chem. 75 (2003) 6068–6076.
[44] Z. Takáts, J.M. Wiseman, B. Gologan, R.G. Cooks, Mass spectrometry sampling under ambient conditions with desorption electrospray ionization, Science 306 (2004) 471–473.
[45] G. Gioumousis, D.P. Stevenson, Reactions of gaseous molecule ions with gaseous molecules. V. Theory, J. Chem. Phys. 29 (1958) 294–299.
[46] T. Su, M.T. Bowers, Ion-polar molecule collisions: the effect of ion size on ion-polar molecule rate constants: the parametrization of the average-dipole-orientation theory, Int. J. Mass Spectrom. Ion Phys. 12 (1973) 347–356.
[47] T.F. Moran, W.H. Hamill, J. Chem. Phys. 39 (1963) 1413.
[48] S.K. Gupta, E.G. Jones, A.G. Harrison, J.J. Myher, Can. J. Chem. 45 (1967) 3107.
[49] D. Smith, M.J. Church, Ion–ion recombination rates in the earth's atmosphere, Planet. Space Sci. 25 (5) (1977) 433–439.
[50] D.G. Samaras, Theory of Ion Flow Dynamics, Dover, New York, 1971, p. 208.
[51] J. Fernández de la Mora, S. Ude, B.A. Thomson, The potential of differential mobility analysis coupled to mass spectrometry for the study of very large singly and multiply charged proteins and protein complexes in the gas phase, Biotechnol. J. 1 (2006) 988–997.
[52] E.W. McDaniel, E.A. Mason, The Mobility and Diffusion of Ions in Gases, Wiley, New York, 1973.
[53] W. Lindinger, A. Hansel, A. Jordan, On-line monitoring of volatile organic compounds at pptv levels by means of proton-transfer-reaction mass-spectrometry (PTR-MS): medical applications, food control, and environmental research, Int. J. Mass Spectrom. Ion Proces. 173 (3) (1998) 191–241.
[54] D. Smith, P. Španel, Selected ion flow tube mass spectrometry (SIFT-MS) for on-line trace gas analysis, Mass Spectrom. Rev. 24(5) (2005) 661–700.
[55] K.G. Asano, D.E. Goeringer, S.A. McLuckey, Parallel monitoring for multiple targeted compounds by ion trap mass spectrometry, Anal. Chem. 67 (17) (2005) 2739–2742.
[56] S.A. McLuckey, D.E. Goeringer, K.G. Asano, G. Vaidyanathan, J.L. Stephenson Jr., High explosives vapor detection by glow discharge-ion trap mass spectrometry, Rapid Commun. Mass Spectrom. 10 (3) (1996) 287–298.
[57] I. Aguirre-de-Carcer, J. Fernández de la Mora, Effect of the background gas on the current emitted from Taylor cones, J. Colloid Interface Sci. 171 (1995) 512–517.
[58] M. Gamero-Castaño, I. Aguirre-de-Carcer, L. de Juan, J. Fernández de la Mora, On the current emitted by Taylor cone-jets of electrolytes in vacuo. Implications for liquid metal ion sources, J. Appl. Phys. 83 (1998) 2428–2434.
[59] R.A. Paz-Schmidt, W. Bonrath, D.A. Plattner, Online ESI-MS analysis of reactions under high pressure, Anal. Chem. 81 (2009) 3665–3668.
[60] L.A. Dillon, V.N. Stone, L.A. Croasdell, P.R. Fielden, N.J. Goddard, C.L. Paul Thomas, Optimization of secondary electrospray ionisation (SESI) for the trace determination of gas-phase volatile organic compounds, Analyst 135 (2) (2010) 306–314.
[61] K.C. Crellin, N. Dalleskab, J.L. Beauchamp, Chemical ionization of the nitrate ester explosives EGDN and PETN by trimethylsilyl cation and comparison of the reactivity of nitrate ester and nitro explosives toward trimethylsilyl cation, Int. J. Mass Spectrom. Ion Process. 165–166 (1997) 641–653.
[62] K.C. Crellin, M. Widmer, J.L. Beauchamp, Chemical ionization of TNT and RDX with trimethylsilyl cation, Anal. Chem. 69 (1997) 1092–1101.
[63] R. Bosque, J. Sales, Polarizabilities of solvents from the chemical composition, J. Chem. Inf. Comput. Sci. 42 (2002) 1154–1163.
[64] http://sparc.chem.uga.edu/sparc/index.cfm?CFID=150493&CFTOKEN=50894148.